Supereruptions in Northwestern Arabia Terra reveal an early stage of Mars's mantle evolution

Authors: Augustus Bates[1]*, S. Goossens[2], J. M. Lorenzo[1], L. Ojha[3], D. R. Hood[4], S. Karunatillake[1], S. Kobs Nawotniak[5], T. Paladino[5]

[1]Department of Geology and Geophysics, Louisiana State University, Baton Rouge, LA, USA

[2] NASA Goddard Space Flight Center

[3]Rutgers, The State University of New Jersey

[4]Baylor University

[5]Idaho State University

*Corresponding author. Email: abate15@lsu.edu

Key Points:

1. Bulk chemistry and geophysical modeling of NW Arabia collectively support resurfacing from volcanic supereruptions.

2. Supereruptions were enriched in large ion lithophiles from low degrees of melting in the Noachian, a previously unknown early stage of interior evolution.

3. Regional chemistry indicates climate-altering supereruptive exhalations of mobile elements like S.

20 **Abstract**

21 Martian meteoritic petrology and regional chemistry of Hesperian-Amazonian volcanism support
22 secularly decreasing degrees of partial melting and thickening crust underlain by simple mantle
23 convection. However, the applicability of this interior evolution model and resurfacing trends to
24 the Noachian remains unknown. Using regional gamma spectroscopy and geophysical analysis,
25 we find that supereruptions characterized Noachian volcanism in NW Arabia with co-enriched
26 K, Th, and Si. Geophysical analysis reveals elastic thickness values below 20 km, indicating a
27 heat flux exceeding many Hesperian volcanoes. Collectively, our results support large ion
28 lithophile loss from low degrees of partial melting of the Noachian mantle, signifying an early
29 stage of interior evolution that contrasts with the Hesperian-Amazonian model. Regional
30 chemistry further suggests climate-altering supereruptive exhalations of $\sim 10^9$ kg S-phases.

31 **Plain Language Summary**

32 The chemical evolution of the martian mantle has long been hypothesized to follow a simple
33 monotonic trend in incompatible elements between the mantle and crust. Since incompatible
34 elements partition into the melt first, on a planet with decreasing partial melting as the crust
35 thickens without recycling (i.e. Mars) the abundance of these elements within extruded rocks
36 would increase with increasing time or volcanic activity. We find that this model oversimplifies
37 the distinctness of the martian mantle during the Noachian. In this study, we show that a
38 Noachian-aged region on Mars exhibits regional geochemical trends that are consistent with
39 explosive igneous activity and that the abundances of incompatible elements (K, Th) within this
40 region suggest low partial melting. We corroborate these findings with estimations of elastic
41 thickness and heat flux in this region.

42

1 Introduction

44   Resurfacing from voluminous, explosive volcanic eruptions can provide compositional

45 insight into mantle-depth geology on Earth (Annen et al., 2006; Reid, 2008). While their martian

46 counterparts during the Noachian may likewise constrain the chemical evolution of the early

47 mantle, they are mostly uncharacterized due to scarce chemical evidence of confirmed Noachian

48 volcanoes (Balta & McSween, 2013; Baratoux et al., 2011). Nevertheless, Noachian

49 supereruptions (eruptions that expel a volume of material exceeding 450 km^3 (Baines & Sparks,

50 2005)) have been hypothesized for Mars (Michalski & Bleacher, 2013) and their existence

51 inferred through observations of expansive friable deposits (Bandfield et al., 2013; Michalski &

52 Bleacher, 2013). Prior works propose super-eruptive paterae in NW Arabia (Michalski &

53 Bleacher, 2013), and mineralogical evidence of their associated eruptions in stratigraphy

54 (Whelley et al., 2021). Notably, these (Kerber et al., 2012; Whelley et al., 2021) are within an

55 igneous chemical province (Taylor et al., 2010) of unknown provenance.

56   The chemistry of any supereruptions would provide a unique perspective into the melt

57 processes of the martian mantle during the Noachian, while advancing prior mantle evolution

58 models that were based on Hesperian-Amazonian regional geochemistry and martian meteorites.

59 Some (i.e., Balta & McSween, 2013; Baratoux et al., 2011), predict an increase in incompatible

60 elements (K, Th) within volcanic deposits through time corresponding to decreasing fractional

61 melting (i.e., degree of partial melting), consequently necessitating highest fractional melting

62 within the martian interior during the Noachian. Contrasting models, primarily based on thermal

63 modelling, suggest rapid cooling of the martian mantle through significant ($> 50\%$) removal of

64 incompatible elements in forming the primary Noachian crust (Grott et al., 2012; Ojha, Karimi,

65 et al., 2019; Plesa et al., 2015), leading to a secular decrease in incompatibles within volcanic

66 deposits. Here we investigate which of these models best explains the geochemistry and

67 geophysical data we have analyzed over NW Arabia.

68

69 **2 Data and Methods**

70   We identify a volcanic supereruption context region (SCR), located within a larger region

71 (that we call broad SCR; BSCR), collectively bound by the chemical province in NW Arabia

72 (Fig. 1). Accordingly, we delineate SCR and BSCR as distinct entities without overlapping

73 chemical map pixels (derived from the Mars Odyssey Gamma Ray Spectroscopy, GRS, spectra),

74 maintaining consistency in mapped geology while also maximizing spatial extent to maintain

75 sufficient coverage (> 10 pixels) for chemical analyses (Boynton et al., 2007; Carnes et al., 2017;

76 Tanaka et al., 2014) (Fig. 1). Such GRS-derived chemical data are ideal for investigating

77 regional trends in the bulk regolith, due to decimeter scale sampling depths and coarse spatial

78 resolution throughout much of the mid-to-low latitudes (about 60º to -60º), with each pixel

79 covering roughly 450 km (Boynton et al., 2007; Hood et al., 2016). While supereruptions could

80 have a dispersed global footprint, SCR and BSCR target the area that would bear the thickest,

81 most weathering-resistant, and compositionally representative units derived from potential

82 supereruptions (Whelley et al., 2021; C. J. N. Wilson, 2008) tied to four putative Noachian

83 paterae (Michalski & Bleacher, 2013).

84   We emphasize regional K-Th and S-Cl concentration trends because these four elements

85 can effectively discriminate among alternative geochemical processes, such as volcanic

86 (Baratoux et al., 2011), subaqueous deposition and alteration (Ehlmann et al., 2011; Taylor et al.,

87 2006), and dust accumulation (Ojha et al., 2018). For example, K and Th fractionation trends can

88 reveal the extent of aqueous alteration of soil and bedrock (basalt) in a region (Sawyer et al.,

89 2000; Taylor et al., 2006, 2010). K and Th are also indicative of volcanic origins because they

90 correlate strongly in igneous rocks as large ion lithophiles (LIL), in part due to their

91 incompatibility with cation sites in silicates (Taylor et al., 2006).

92   We also compare S and Cl trends, because they are present in volatile phases of terrestrial

93 volcanic degassing and may function similarly on Mars (Diez et al., 2009; Gaillard & Scaillet,

94 2009; Keller et al., 2006; Ojha et al., 2018; Ojha, Karunatillake, et al., 2019). As key volatiles,

95 they can serve as a proxy for eruptive explosivity, and offer insight into mantle pressure regimes

96 (Baratoux et al., 2011; Burton et al., 2009; Gasnault et al., 2010; Hood et al., 2016; Ojha et al.,

97   2018; Ojha, Karunatillake, et al., 2019; Spilliaert et al., 2006; Taylor et al., 2010). Furthermore,

98   S and Cl have been used to characterize a global dust source region for Mars, through their

99   consistent molar ratio observed in situ and within heavily mantled locales (Berger et al., 2016;

100 Kerber et al., 2011; Ojha et al., 2018).

101   We complement our geochemical analyses with geophysical results from gravity and

102 topography to estimate load density and elastic thickness of the lithosphere within SCR. Elastic

103 thickness is a key parameter, as it represents the thickness of the deformable lithosphere, a proxy

104 for heat flow and how coupled the lithosphere is to the mantle. As such, elastic thickness can

105 offer insight into the thermal environment of a region (Belleguic et al., 2005; Grott & Wieczorek,

106 2012; McGovern et al., 2004) and the density of the crustal load provides insight into its

107 composition (Ojha & Lewis, 2018).

108   Our investigations of regional geochemistry involve comparative analysis between SCR

109 and other geologically unique regions on Mars. However, instead of an exhaustive set of regional

110 chemical references, we consider specific regions which are geographically distributed for

111 chemical comparisons (Fig. 1). This is because the early geologic history of Mars is difficult to

112 interpret due to diverse chemical overprinting resulting from a multitude of processes, including

113 magmatism (Balta & McSween, 2013; Baratoux et al., 2011, 2013), dust transport (Ojha et al.,

114 2018) and aqueous alteration (Bibring et al., 2006; Ehlmann et al., 2011). Our comparative

115 region selections maximize insight from diverse subaerial sedimentary and igneous processes

116 and minimize bias from chemical overprinting across proximal regions (Table 1). We delineate

117 these regions following topography and mapped geology (Tanaka et al., 2014) and compare

118 subsequently using GRS-derived geochemistry.

3 Results and Discussion

119

120   The K and Th trends (Fig. 2A) within SCR are most consistent with igneous

121 geochemistry of an enriched mantle source (Hefferan & O'Brien, 2010). SCR has the highest

122 mean value of K and Th compared to the reference regions, a much lower dispersion in overall K

123 and Th abundances in comparison to similarly enriched regions (i.e. Isidis and Apollinaris

124 Mons), and a K/Th ratio resembling the crustal average (Table 1). A supereruption within SCR

125 would have rapidly exhausted the source magma and terminated melting over a relatively short

126 timescale (Scott et al., 2001). SCR's limited dispersion in K and Th (Fig. 2A) is consistent with

127 fast and voluminous igneous emplacement. In contrast, the large dispersion in Th and lower

128 abundances of K and Th observed for Apollinaris correspond to its ~2 Ma eruptive life (Robbins

129 et al., 2011) that may span a chemical transition in the martian mantle (Balta & McSween, 2013).

130   The fast and voluminous emplacement indicated by the K and Th trends within SCR is

131 unique among other regions on Mars. For example, our volcanic reference regions all appear to

132 exhibit Th abundances consistent with mantle evolution models that suggest increasing

133 abundances of incompatible elements with increasingly younger instances of magmatism (Fig.

134 2A, Table 1) (Balta & McSween, 2013; Baratoux et al., 2011). These volcanoes also have K/Th

135 mass ratios that resemble the crustal average more than sedimentary references, though some

136 variability in overall abundances of K and Th among the volcanic references is also evident. K

137 and Th abundances are affected by the hydration state of the mantle (Balta & McSween, 2013),

138 by variations in chemistry and melt processes of martian mantle sources driven in part by

139 enriched pockets of residual melt near the crust mantle boundary (Basu Sarbadhikari et al.,

140 2017), or by differing melt conditions (Baratoux et al., 2011; Hefferan & O'Brien, 2010). While

141 these mechanisms may result in K/Th ratios that are distinct from the global spatial correlation,

142   K and Th abundances that strongly diverge from global linearity are generally due to secondary

143   alteration (Taylor et al., 2006). This phenomenon is especially noticeable in our sedimentary

144   reference regions (Fig. 2A), which consistently show a weaker bivariate correlation between K

145   and Th, possibly from chemical weathering of igneous material that initially constituted the basin

146   floors (Ehlmann et al., 2011; Taylor et al., 2006; Zalewska, 2013). In addition, our sedimentary

147   references have K/Th ratios significantly above the crustal average (Table 1), consistent with

148   low-pH alteration (Taylor et al., 2006; Zalewska, 2013).

149   Martian dust is enriched in S and Cl (Berger et al., 2016) and has been shown to exhibit a

150   consistent molar ratio of S/Cl (Ojha et al., 2018), distinct from volcanic degassing (Gaillard &

151   Scaillet, 2009; King & McLennan, 2010; Ojha et al., 2018; Ojha, Karunatillake, et al., 2019).

152   Our calculated mean molar S/Cl ratio for SCR (~4.6) does not fall within the global dust molar

153   ratio range (3.0 – 4.4) (Table 1; (Ehlmann et al., 2011; Kerber et al., 2011). The observed S

154   enrichment in SCR (Fig. 2B), coupled with a S/Cl molar ratio diverging from that of martian dust

155   (Ojha et al., 2018), supports sulfur adsorbed or chemically bound in the soil and regolith from

156   volcanic degassing (Bibring et al., 2006; Ojha, Karunatillake, et al., 2019). Si and K abundances

157   can provide additional corroboration, as dust mantled areas are generally depleted in these

158   elements relative to the average crust (Berger et al., 2016; Lasue et al., 2018; Viviano et al.,

159   2019). SCR is enriched in both Si and K (SI Appendix, Fig. S2) compared to the crust, further

160   discounting compositional contributions from dust mantling within SCR.

161   Localized chemical weathering of basalt is unlikely to substantially enrich S and Cl (Diez

162   et al., 2009). This is best exhibited in our Eridania reference, composed primarily of weathered

163   volcanic material (Tanaka et al., 2014), exhibiting one of the lowest overall abundances of S and

164   Cl reported in this study (Fig. 2B). Conversely, the Medusae Fossae Formation (MFF) has the

165   highest observed S and Cl values in this study (Fig. 2B), associated with its origin as a

166   pyroclastic deposit from massive eruptions (Diez et al., 2009; Ojha & Lewis, 2018). This makes

167   the MFF's S and Cl abundances key references for extensive explosive eruptions enhancing the

168   volatile content of a region (Diez et al., 2009; Ojha et al., 2018). SCR is second in overall S and

169   Cl abundances to Apollinaris (and by extension the MFF), which offers further support of

170   volcanic degassing being the primary mechanism to enhance S and Cl within SCR (Diez et al.,

171   2009; Ojha et al., 2018). Nevertheless, the distinctness in S/Cl ratios between SCR and MFF

172   suggest that the pyroclastic deposits that may constitute SCR's chemistry do not serve as a major

173   source of martian dust.

174   The observed S trends within SCR are consistent with K and Th trends, indicating that

175   SCR's chemistry is not the result of aqueous alteration, despite a considerable enrichment in H_2O

176   (SI Appendix, Fig. S2). If SCR hosted abundant fluvial activity, as its H_2O abundance may

177   superficially suggest, S-phases would have been mobilized through interaction with water,

178   resulting in substantial acidic weathering during the Middle to Late Noachian. Such sulfate-

179   driven alteration is typically associated with ancient ground water systems on Mars (Zalewska,

180   2013), which would fractionate Th from K at low pH (Sawyer et al., 2000; Taylor et al., 2006).

181   This would enrich the residual minerals in K, resulting in a K/Th ratio higher than that of the

182   crust (Taylor et al., 2006), which is not observed at SCR (Table 1). In contrast, a high K/Th ratio

183   is observed for Hellas, consistent with regional aqueous alteration within the basin (Zalewska,

184   2013). SCR shows little chemical similarity to Hellas within the scope of this study (Figs. 2 and

185   3), suggesting that SCR's observed S abundances are unrelated to sulfate deposits in aqueous

186   (e.g., fluvial, playa, lacustrine) settings. There are many mechanisms which could have

187   influenced SCR's H_2O abundance, such as pyroclastic scavenging of atmospheric vapor, which

188 is primarily dictated by particle fall time through the atmosphere (Wilson & Head, 2007).

189 Consequently, the simultaneous enrichment of H_2O along with S and Cl, given the rest of the

190 chemical context of SCR, is more consistent with a highly explosive volcanic provenance.

191 Geophysical modeling also supports the geochemical evidence for SCR's supereruptive

192 provenance. We use admittance analysis from gravity and topographic data to provide estimates

193 of the elastic thickness of the lithosphere and a range of potential densities for the loads (see SI

194 for details). We use elastic thickness estimates as proxies for regional thermal flux (Belleguic et

195 al., 2005; McGovern et al., 2004), which has implications for SCR's inferred eruptive regime.

196 SCR's low elastic thickness of ~15 km (Fig. 3) roughly corresponds to a thermal gradient

197 exceeding 19 K/km and a heat flux between 47 and 75 mW/m^2, a range higher than for some

198 martian volcanoes (Karimi et al., 2016; McGovern et al., 2004). This estimate resembles prior

199 heat flow estimates (Belleguic et al., 2005; McGovern et al., 2004) which report similar elastic

200 thickness values within the Arabia region. The increased thermal flux associated with

201 predominantly low elastic thickness values for SCR is in turn consistent with both a mantle

202 plume beneath SCR and enrichment of radioactive elements like K and Th (Michael, 1995).

203 Our geophysical analyses also yield a load density for SCR resembling the low densities

204 for MFF (Ojha & Lewis, 2018), consistent with thick pyroclastic deposits. The regional load

205 density as obtained from gravity and topography (Fig. 3; SI Appendix, Fig. S3) is on average

206 lower than 1900 kg/m^3. Deposition of friable material derived from supereruptions with

207 associated low top load density can arise from more buoyant magma containing dissolved gases

208 (McSween Jr., 1994). Our estimated load density also constrains the amount of degassed sulfur

209 from eruptions. Using the erupted volume estimated for one patera within SCR by (Michalski &

210 Bleacher, 2013), and an average density of 1800 kg/m^3 (Fig. 3), we estimate a 12×10^9 kg

211   maximum mass of erupted material. Of this total mass, approximately 2.8×10^8 kg is sulfur,

212   based on our measured S abundances within SCR (averaging 2.4 wt%; Table 1). If this mass

213   represents the 30% which was scavenged by ash, a percentage consistent with conservative

214   estimates of atmospheric degassing (Ojha, Karunatillake, et al., 2019), the remaining mass of

215   sulfur degassed to the atmosphere is approximately 6.5×10^8 kg. Considering all four paterae

216   with volumetrically similar concurrent eruptions, the amount of degassed sulfur increases to 2.6

217    $\times 10^9$ kg. For comparison, the Toba eruption, the largest Quaternary volcanic eruption on Earth,

218   emitted 10^{10}-10^{12} kg of sulfur (c.f. Ojha et al., 2018). If eruptions within SCR were brief and

219   clustered temporally, such amounts of degassed sulfur alone would have impacted global climate

220   (Halevy et al., 2007; Rampino & Self, 1992; Tian et al., 2010).

221   Given the evidence for volcanogenic Cl and S within SCR, the mantle context of the

222   eruptions can also be considered. The average elemental abundances of S and Cl within SCR ($\geq$

223   3wt%; Table 1) suggest that the magma source had a relatively high abundance of dissolved

224   volatiles, which would lead to explosive eruptions that rival terrestrial supereruptions (Hefferan

225   & O'Brien, 2010; Spilliaert et al., 2006). Shallow melting of even a dry mantle source can

226   produce S-enriched magma, as S exsolves into the vapor phase at low pressures within drier

227   magmas, also increasing the potential for explosive eruptions (Burton et al., 2009; Spilliaert et

228   al., 2006). In addition, we observe an enrichment in Ca (SI Appendix, Fig. S2), consistent with

229   more Ca-rich pyroxenes within the primary melt at this time relative to succeeding eons

230   (Baratoux et al., 2013). We also observe a Si enrichment (SI Appendix, Fig. S2) within SCR

231   which would cause the high melt viscosities implied for older, more explosive volcanism

232   (Baratoux et al., 2011). SCR additionally exhibits similar degrees of enrichment in K and Cl

233   compared to the martian crust (SI Appendix, Fig. S2), consistent with their typical correlation

234   within terrestrial basalts (Workman et al., 2006).

235   Based on a Middle Noachian age for SCR, any eruptions were likely sourced from a

236   hotter mantle with less confining pressure (Baratoux et al., 2011). This would suggest that any

237   eruptions would have high degrees of partial melting (Baratoux et al., 2011), which contrasts

238   with the observed abundances of K and Th (Fig. 2). However, large ion lithophile abundance

239   may not be as representative of the chemical evolution of the martian mantle through time as

240   posited by some mantle evolution models (i.e, Balta & McSween, 2013; Baratoux et al., 2011).

241   Younger and older volcanoes differ categorically in Si abundance, but Th and Fe abundances

242   overlap among age groups (Baratoux et al., 2011; Hahn, B C, Mclennan, 2007). Since Th

243   abundance is inversely related to the amount of partial melting prior to eruption, the overlap in

244   Th abundance among older and younger volcanoes reveals that partial melting may not follow a

245   monotonic temporal trend. This contradicts the predictions of key petrologically-based mantle

246   evolution models (i.e., Balta & McSween, 2013; Baratoux et al., 2011) from regional and

247   meteoritic geochemistry.

248   The observed compositional trends provide additional insight on an evolving mantle

249   composition. If eruptive chemistry primarily represents sampling of a heterogeneous martian

250   crust, consistent trends in Si and Th with age become less likely, as Hesperian to Amazonian

251   volcanic provinces are not collocated, and therefore must be sampling the crust at different

252   depths and in different ways (Annen et al., 2006). Indeed, on Earth, the intermingling of residual

253   melt and crustal melt is responsible for much of the observed heterogeneity among surface

254   expressions of magmatism (Annen et al., 2006). However, on Mars, crustal compositional

255   heterogeneity is subdued compared to Earth (Baratoux et al., 2014), and the mantle is considered

256   generally less dynamic (Ruiz et al., 2011), suggesting that eruptive chemical changes are

257   primarily driven by changing mantle composition (Balta & McSween, 2013). Thus, the

258   temporally consistent trend in Si likely reflects a changing mantle composition wherein magmas

259   experience similar degrees of compositional dilution from crustal assimilation, likely due to a

260   substantially thick crust, among post-Noachian, martian volcanoes. Our study shows that SCR

261   has the thermal properties of Noachian volcanoes (Fig. 3) (Baratoux et al., 2011; McGovern et

262   al., 2004), but with a surface chemistry that is unique (Fig. 2). This chemistry indicates a

263   compositionally distinct mantle source among contemporaneous volcanoes, capable of producing

264   explosive eruptions.

265   **4 Conclusions**

266   From our collective observations, we hypothesize that a massive, volatile-enriched,

267   mantle plume underwent low fractional melting (Workman et al., 2006) in the Noachian to yield

268   a regional magma body, enriched in LILs like K and Th. Low fractional melting is imperative to

269   cause SCR's Th enrichment, unlike the sometimes lower Th across older volcanic provinces

270   compared to younger counterparts (Balta & McSween, 2013; Baratoux et al., 2011). The

271   deviation from the temporal trend in Th used in prior mantle evolution models would be

272   consistent with SCR's distinctness compared to other volcanic provinces, as reflected in

273   supereruptions (Gravley et al., 2016; Reid, 2008; Taylor et al., 2010). The possibility of

274   explosive eruptions from Si and volatile (S, Cl) enriched Noachian melts is broadly consistent

275   with geomorphic and thermophysical evidence of explosive volcanic resurfacing in the Noachian

276   (Bandfield et al., 2013). Low confining pressure from a thermally eroded local lithosphere – as

277   consistent with our geophysical analyses – may have further enhanced explosivity.

278   The temporally and spatially localized explosive eruptions we infer early in martian

279   history are consistent with massive, climate-transforming, volatile injections into the atmosphere

280   (Ojha, Karunatillake, et al., 2019). If such eruptions were pervasive during the Noachian, it

281   would dramatically affect the stability and availability of water on the martian surface (Halevy et

282   al., 2007; Tian et al., 2010). The possible onset of glaciation from the explosive eruptions and

283   sulfur degassing (Halevy et al., 2007; Tian et al., 2010) within SCR would affect surface

284   habitability, likely driving those habitable zones underground where it was warmer. Furthermore,

285   the regional magma body that fed eruptions within SCR likely remained thermally active long

286   after the termination of surface volcanism (Annen & Sparks, 2002). Deep crustal intrusion zones,

287   such as the one we hypothesize for SCR, can take millions of years to return to the global

288   geothermal gradient state (Annen & Sparks, 2002). Future investigations of the larger chemical

289   province that houses SCR focused on regolith mixing processes would help deconvolve varying

290   compositional input from the diverse geologic units in the area. The contrast in SCR's chemistry

291   with key models of martian mantle evolution (Balta & McSween, 2013; Baratoux et al., 2011),

292   also reinforces regional heterogeneity in mantle processes and makes NW Arabia an ideal

293   endmember to refine the models.

294
295
296

308 **Competing interests:** Authors declare that they have no competing interests.

309

310 **Data and materials availability:** Mapped geology for Mars was acquired from the USGS
311 archive (https://pubs.usgs.gov/sim/3292/) developed by Tanaka et al., (2014) and subsequent
312 analysis of this data was performed using ArcGIS software. GRS spectra are from the NASA
313 Planetary Database System (PDS, https://pds-
314 geosciences.wustl.edu/missions/odyssey/grs_cgs.html). Topographic data are from the Mars
315 Orbiter Laser Altimeter (MOLA) data, also archived at NASA PDS, and used in the
316 MarsTopo2600 model (Wieczorek, 2015, see
317 https://figshare.com/articles/dataset/Spherical_harmonic_model_of_the_shape_of_Mars_MarsTo
318 po2600/12402653). The gravity model used in our analysis can be found at the NASA/GSFC
319 PGDA website (https://pgda.gsfc.nasa.gov/products/63). Details of data sources follow in their
320 respective sections.

321 **Supplementary Materials**

322 Materials and Methods

323 Supplementary Text

324 Figs. S1 to S3

325 Table S1

326 References (*1-44*)

327

328

329

References

Annen, C., & Sparks, R. S. J. (2002). Effects of repetitive emplacement of basaltic intrusions on thermal evolution and melt generation in the crust. *Earth and Planetary Science Letters*, *203*(3–4), 937–955. https://doi.org/10.1016/S0012-821X(02)00929-9

Annen, C., Blundy, J. D., & Sparks, R. S. J. (2006). The genesis of intermediate and silicic magmas in deep crustal hot zones. *Journal of Petrology*, *47*(3), 505–539. https://doi.org/10.1093/petrology/egi084

Baines, P. G., & Sparks, R. S. J. (2005). Dynamics of giant volcanic ash clouds from supervolcanic eruptions. *Geophysical Research Letters*, *32*(24), 1–4. https://doi.org/10.1029/2005GL024597

Balta, J. B., & McSween, H. Y. (2013). Water and the composition of Martian magmas. *Geology*, *41*(July), 1115–1118. https://doi.org/10.1130/G34714.1

Bandfield, J. L., Edwards, C. S., Montgomery, D. R., & Brand, B. D. (2013). The dual nature of the martian crust: Young lavas and old clastic materials. *Icarus*, *222*(1), 188–199. https://doi.org/10.1016/j.icarus.2012.10.023

Baratoux, D., Toplis, M. J., Monnereau, M., & Gasnault, O. (2011). Thermal history of Mars inferred from orbital geochemistry of volcanic provinces. *Nature*, *472*(7343), 338–41. https://doi.org/10.1038/nature09903

Baratoux, D., Toplis, M. J., Monnereau, M., & Sautter, V. (2013). The petrological expression of early Mars volcanism. *Journal of Geophysical Research E: Planets*, *118*(1), 59–64. https://doi.org/10.1029/2012JE004234

Baratoux, D., Samuel, H., Michaut, C., Toplis, M. J., Monnereau, M., Wieczorek, M., et al. (2014). Petrological constraints on the density of the Martian crust. *Journal of Geophysical*

353 *Research*, *119*, 1707–1727. https://doi.org/10.1002/2014JE004642

354 Basu Sarbadhikari, A., Babu, E. V. S. S. K., & Vijaya Kumar, T. (2017). Chemical layering in

355 the upper mantle of Mars: Evidence from olivine-hosted melt inclusions in Tissint.

356 *Meteoritics and Planetary Science*, *52*(2), 251–267. https://doi.org/10.1111/maps.12790

357 Belleguic, V., Lognonné, P., & Wieczorek, M. (2005). Constraints on the Martian lithosphere

358 from gravity and topography data. *Journal of Geophysical Research E: Planets*, *110*(11), 1–

359 22. https://doi.org/10.1029/2005JE002437

360 Berger, J. A., Schmidt, M. E., Gellert, R., Campbell, J. L., King, P. L., Flemming, R. L., et al.

361 (2016). A global Mars dust composition refined by the Alpha-Particle X-ray Spectrometer

362 in Gale Crater. *Geophysical Research Letters*, *43*(1), 67–75.

363 https://doi.org/10.1002/2015GL066675

364 Bibring, J.-P., Langevin, Y., Mustard, J. F., Poulet, F., Arvidson, R., Gendrin, A., et al. (2006).

365 Global mineralogical and aqueous mars history derived from OMEGA/Mars Express data.

366 *Science (New York, N.Y.)*, *312*(5772), 400–404. https://doi.org/10.1126/science.1122659

367 Boynton, W. V., Taylor, G. J., Evans, L. G., Reedy, R. C., Starr, R., Janes, D. M., et al. (2007).

368 Concentration of H, Si, Cl, K, Fe, and Th in the low- and mid-latitude regions of Mars.

369 *Journal of Geophysical Research*, *112*, E12S99. https://doi.org/10.1029/2007JE002887

370 Burton, M. R., Caltabiano, T., Murè, F., Salerno, G., & Randazzo, D. (2009). SO2 flux from

371 Stromboli during the 2007 eruption: Results from the FLAME network and traverse

372 measurements. *Journal of Volcanology and Geothermal Research*, *182*(3–4), 214–220.

373 https://doi.org/10.1016/j.jvolgeores.2008.11.025

374 Carnes, L. L., Karunatillake, S., Susko, D. A., & Hood, D. R. (2017). Delineating the Arabia

375 Terra region on Mars to investigate paterae orgins. In *LPSC2017* (p. Abstract 1756).

376   https://doi.org/10.1038/ngeo2845

377 Diez, B., Feldman, W. C., Mangold, N., Baratoux, D., Maurice, S., Gasnault, O., et al. (2009).

378   Contribution of Mars Odyssey GRS at Central Elysium Planitia. *Icarus*, *200*(1), 19–29.

379   https://doi.org/10.1016/j.icarus.2008.11.011

380 Ehlmann, B. L., Mustard, J. F., Murchie, S. L., Bibring, J.-P., Meunier, A., Fraeman, A. a, &

381   Langevin, Y. (2011). Subsurface water and clay mineral formation during the early history

382   of Mars. *Nature*, *479*(7371), 53–60. https://doi.org/10.1038/nature10582

383 Gaillard, F., & Scaillet, B. (2009). The sulfur content of volcanic gases on Mars. *Earth and*

384   *Planetary Science Letters*, *279*(1–2), 34–43. https://doi.org/10.1016/j.epsl.2008.12.028

385 Gasnault, O., Jeffrey Taylor, G., Karunatillake, S., Dohm, J., Newsom, H., Forni, O., et al.

386   (2010). Quantitative geochemical mapping of martian elemental provinces. *Icarus*, *207*(1),

387   226–247. https://doi.org/10.1016/j.icarus.2009.11.010

388 Gravley, D. M., Deering, C. D., Leonard, G. S., & Rowland, J. V. (2016). Ignimbrite flare-ups

389   and their drivers: A New Zealand perspective. *Earth-Science Reviews*, *162*, 65–82.

390   https://doi.org/10.1016/j.earscirev.2016.09.007

391 Grott, M., & Wieczorek, M. A. (2012). Density and lithospheric structure at Tyrrhena Patera,

392   Mars, from gravity and topography data. *Icarus*, *221*(1), 43–52.

393   https://doi.org/10.1016/j.icarus.2012.07.008

394 Grott, M., Baratoux, D., Hauber, E., Sautter, V., Mustard, J. F., Gasnault, O., et al. (2012). Long-

395   Term Evolution of the Martian Crust-Mantle System. *Space Science Reviews*, *174*(1–4), 49–

396   111. https://doi.org/10.1007/s11214-012-9948-3

397 Hahn, B C, Mclennan, S. M. (2007). Evolution and Geochemistry of the Martian Crust:

398   Integrating Mission Datasets. In *Seventh International Conference on Mars*. Pasadena, CA:

399   Lunar and Planetary Institute. Retrieved from

400   https://www.lpi.usra.edu/meetings/7thmars2007/pdf/3179.pdf

401 Halevy, I., Zuber, M. T., & Schrag, D. P. (2007). A Sulfur Dioxide Climate Feedback on Early

402   Mars. *Science*, *318*(December), 1903–1908. https://doi.org/10.5040/9780755621101.0007

403 Hefferan, K., & O'Brien, J. (2010). Magma and Intrusive Structures. In *Earth Materials* (1st ed.,

404   pp. 212–227). John Wiley & Sons, Ltd.

405 Hood, D. R., Judice, T., Karunatillake, S., Rogers, D., Dohm, J. M., Susko, D. A., & Carnes, L.

406   K. (2016). Assessing the geologic evolution of Greater Thaumasia, Mars. *Journal of*

407   *Geophysical Research: Planets*, *121*(9), 1753–1769. https://doi.org/10.1002/2016JE005046

408 Karimi, S., Dombard, A. J., Buczkowski, D. L., Robbins, S. J., & Williams, R. M. (2016). Using

409   the viscoelastic relaxation of large impact craters to study the thermal history of Mars.

410   *Icarus*, *272*, 102–113. https://doi.org/10.1016/j.icarus.2016.02.037

411 Keller, J. M., Boynton, W. V., Karunatillake, S., Baker, V. R., Dohm, J. M., Evans, L. G., et al.

412   (2006). Equatorial and midlatitude distribution of chlorine measured by Mars Odyssey

413   GRS. *Journal of Geophysical Research*, *112*(E3), E03S08.

414   https://doi.org/10.1029/2006JE002679

415 Kerber, L., Head, J. W., Madeleine, J. B., Forget, F., & Wilson, L. (2011). The dispersal of

416   pyroclasts from Apollinaris Patera, Mars: Implications for the origin of the Medusae Fossae

417   Formation. *Icarus*, *216*(1), 212–220. https://doi.org/10.1016/j.icarus.2011.07.035

418 Kerber, L., Head, J. W., Madeleine, J.-B., Forget, F., & Wilson, L. (2012). The dispersal of

419   pyroclasts from ancient explosive volcanoes on Mars: Implications for the friable layered

420   deposits. *Icarus*, *219*(1), 358–381. https://doi.org/10.1016/j.icarus.2012.03.016

421 King, P. L., & McLennan, S. M. (2010). Sulfur on Mars. *Elements*, *6*(2), 107–112.

422   https://doi.org/10.2113/gselements.6.2.107

423   Lasue, J., Cousin, A., Meslin, P. Y., Mangold, N., Wiens, R. C., Berger, G., et al. (2018).

424   Martian Eolian Dust Probed by ChemCam. *Geophysical Research Letters*, *45*(20), 10,968-

425   10,977. https://doi.org/10.1029/2018GL079210

426   McGovern, P. J., Solomon, S. C., Smith, D. E., Zuber, M. T., Simons, M., Wieczorek, M. A., et

427   al. (2004). Correction to "Localized gravity/topography admittance and correlation spectra

428   on Mars: Implications for regional and global evolution." *Journal of Geophysical Research*

429   *E: Planets*, *109*(12), 19–1. https://doi.org/10.1029/2002je001854

430   McSween Jr., H. Y. (1994). What we have learned about Mars from SNC meteorites.

431   *Meteoritics*, *29*(1 994), 757–779. Retrieved from

432   http://articles.adsabs.harvard.edu/full/thumbnails/seri/Metic/0029/1994Metic..29..757M.htm

433   l

434   Michael, P. (1995). Regionally distinctive sources of depleted MORB: Evidence from trace

435   elements and H2O. *Earth and Planetary Science Letters*, *131*(3–4), 301–320.

436   https://doi.org/10.1016/0012-821X(95)00023-6

437   Michalski, J. R., & Bleacher, J. E. (2013). Supervolcanoes within an ancient volcanic province in

438   Arabia Terra, Mars. *Nature*, *502*(7469), 47–52. https://doi.org/10.1038/nature12482

439   Ojha, L., & Lewis, K. (2018). The Density of the Medusae Fossae Formation: Implications for

440   its Composition, Origin, and Importance in Martian History. *Journal of Geophysical*

441   *Research: Planets*, *123*(6), 1368–1379. https://doi.org/10.1029/2018JE005565

442   Ojha, L., Lewis, K., Karunatillake, S., & Schmidt, M. (2018). The Medusae Fossae Formation as

443   the single largest source of dust on Mars. *Nature Communications*, *9*(1), 1–7.

444   https://doi.org/10.1038/s41467-018-05291-5

445   Ojha, L., Karunatillake, S., & Lacovino, K. (2019). Atmospheric Injection of Sulfur from the

446   Medusae Fossae Forming Events. *Planetary and Space Science*, *179*, 104734.

447   https://doi.org/10.1016/j.pss.2019.104734

448   Ojha, L., Karimi, S., Lewis, K. W., Smrekar, S. E., & Siegler, M. (2019). Depletion of Heat

449   Producing Elements in the Martian Mantle. *Geophysical Research Letters*, *46*(22), 12756–

450   12763. https://doi.org/10.1029/2019GL085234

451   Plesa, A. C., Tosi, N., Grott, M., & Breuer, D. (2015). Thermal evolution and Urey ratio of Mars.

452   *Journal of Geophysical Research: Planets*, *120*(5), 995–1010.

453   https://doi.org/10.1002/2014JE004748

454   Rampino, M. R., & Self, S. (1992). Volcanic Winter and Accelerated Glaciation Following the

455   Toba Super-Eruption. *Nature*, *359*(September), 50–52.

456   Reid, M. R. (2008). How long does it take to supersize an eruption. *Elements*, *4*(1), 23–28.

457   https://doi.org/10.2113/GSELEMENTS.4.1.23

458   Robbins, S. J., Di Achille, G., & Hynek, B. M. (2011). The volcanic history of Mars: High-

459   resolution crater-based studies of the calderas of 20 volcanoes. *Icarus*, *211*(2), 1179–1203.

460   https://doi.org/10.1016/j.icarus.2010.11.012

461   Ruiz, J., McGovern, P. J., Jiménez-Díaz, A., López, V., Williams, J.-P., Hahn, B. C., & Tejero,

462   R. (2011). The thermal evolution of Mars as constrained by paleo-heat flows. *Icarus*,

463   *215*(2), 508–517. https://doi.org/10.1016/j.icarus.2011.07.029

464   Sawyer, D. J., McGehee, M. D., Canepa, J., & Moore, C. B. (2000). Water soluble ions in the

465   Nakhla martian meteorite. *Meteoritics and Planetary Science*, *35*(4), 743–747.

466   https://doi.org/10.1111/j.1945-5100.2000.tb01458.x

467   Scott, E. D., Wilson, L., & Head, J. W. (2001). Evidence for episodicity in the magma supply to

468   the large Tharsis Volcanoes. *Journal Geophysical Research*, *106*, 1423–1433.

469   Spilliaert, N., Allard, P., Métrich, N., & Sobolev, A. V. (2006). Melt inclusion record of the

470   conditions of ascent, degassing, and extrusion of volatile-rich alkali basalt during the

471   powerful 2002 flank eruption of Mount Etna (Italy). *Journal of Geophysical Research:*

472   *Solid Earth*, *111*(4). https://doi.org/10.1029/2005JB003934

473   Tanaka, K. L., Robbins, S. J., Fortezzo, C. M., Skinner, J. A., & Hare, T. M. (2014). The digital

474   global geologic map of Mars: Chronostratigraphic ages, topographic and crater morphologic

475   characteristics, and updated resurfacing history. *Planetary and Space Science*, *95*, 11–24.

476   https://doi.org/10.1016/j.pss.2013.03.006

477   Taylor, G. J., Stopar, J. D., Boynton, W. V., Karunatillake, S., Keller, J. M., Brückner, J., et al.

478   (2006). Variations in K/Th on Mars. *Journal of Geophysical Research*, *112*(E3), E03S06.

479   https://doi.org/10.1029/2006JE002676

480   Taylor, G. J., Martel, L. M. V., Karunatillake, S., Gasnault, O., & Boynton, W. V. (2010).

481   Mapping Mars geochemically. *Geology*, *38*(2), 183–186. https://doi.org/10.1130/G30470.1

482   Tian, F., Claire, M. W., Haqq-Misra, J. D., Smith, M., Crisp, D. C., Catling, D., et al. (2010).

483   Photochemical and climate consequences of sulfur outgassing on early Mars. *Earth and*

484   *Planetary Science Letters*, *295*(3–4), 412–418. https://doi.org/10.1016/j.epsl.2010.04.016

485   Viviano, C., Murchie, S. L., Daubar, I. J., Morgan, M. F., Seelos, F. P., & Plescia, J. B. (2019).

486   Composition of Amazonian volcanic materials in Tharsis and Elysium, Mars, from

487   MRO/CRISM reflectance spectra. *Icarus*, #pagerange#.

488   https://doi.org/10.1016/j.icarus.2019.03.001

489   Whelley, P., Matiella Novak, A., Richardson, J., Bleacher, J., Mach, K., & Smith, R. N. (2021).

490   Stratigraphic Evidence for Early Martian Explosive Volcanism in Arabia Terra.

491   *Geophysical Research Letters*, *48*(15), 1–12. https://doi.org/10.1029/2021gl094109

492   Wieczorek, M. A. (2008). Constraints on the composition of the martian south polar cap from

493   gravity and topography. *Icarus*, *196*(2), 506–517.

494   https://doi.org/10.1016/j.icarus.2007.10.026

495   Wilson, C. J. N. (2008). Supereruptions and supervolcanoes: Processes and products. *Elements*,

496   *4*(1), 29–34. https://doi.org/10.2113/GSELEMENTS.4.1.29

497   Wilson, L., & Head, J. W. (2007). Explosive volcanic eruptions on Mars: Tephra and

498   accretionary lapilli formation, dispersal and recognition in the geologic record. *Journal of*

499   *Volcanology and Geothermal Research*, *163*(1–4), 83–97.

500   https://doi.org/10.1016/j.jvolgeores.2007.03.007

501   Workman, R. K., Hauri, E., Hart, S. R., Wang, J., & Blusztajn, J. (2006). Volatile and trace

502   elements in basaltic glasses from Samoa: Implications for water distribution in the mantle.

503   *Earth and Planetary Science Letters*, *241*(3–4), 932–951.

504   https://doi.org/10.1016/j.epsl.2005.10.028

505   Zalewska, N. (2013). Hellas Planitia as a potential site of sedimentary minerals. *Planetary and*

506   *Space Science*, *78*, 25–32. https://doi.org/10.1016/j.pss.2012.12.006
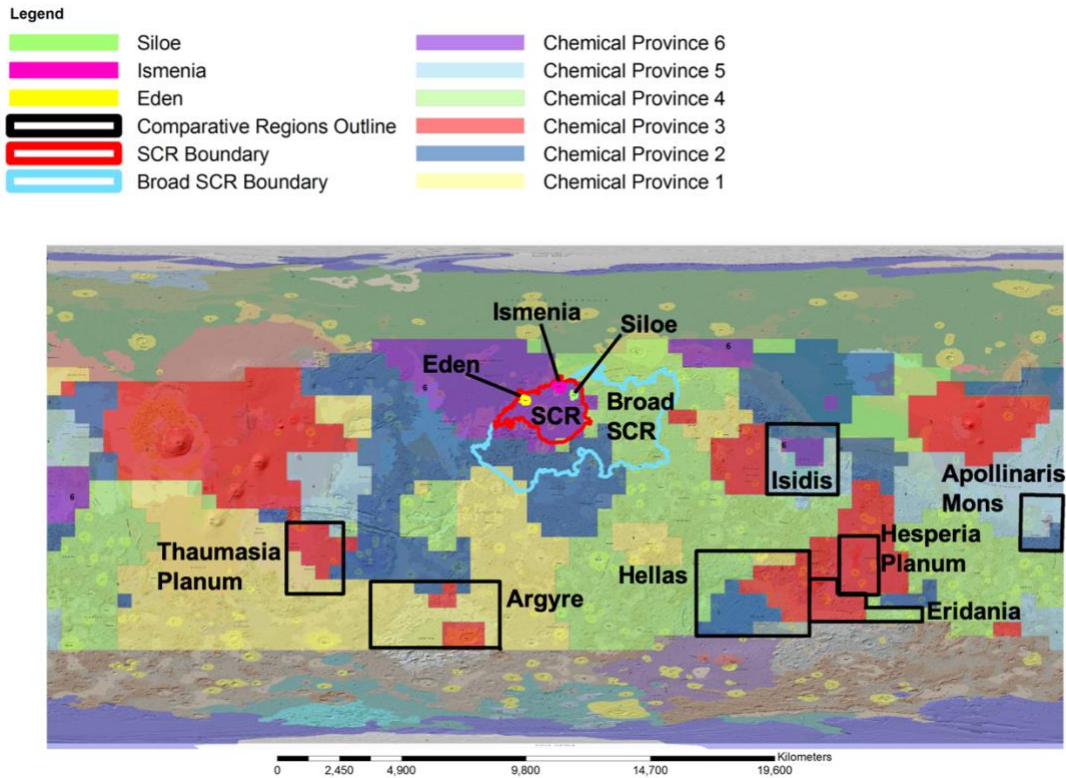
507

508

509

Fig. 1: Geologic map of Mars (Tanaka et al., 2014) with Taylor et al.'s geochemical provinces (Taylor et al., 2010) overlain. SCR and BSCR derived by us are shown along with three previously proposed paterae (Siloe, Ismenia, and Eden) by (Michalski & Bleacher, 2013). We delineated SCR using a combination of mapped geology, regional chemistry and topography, to ensure that geologic and chemical consistency within SCR was maintained. Thus, SCR is composed entirely of chemical Province 6 by (Taylor et al., 2010). BSCR represents the more heterogeneous Arabia region that surrounds SCR, which was also delineated using mapped geology, chemistry and topography. The black boxes outline comparative regions for compositional study. Our basin references are Argyre, Hellas and Isidis. Our volcanic references are Thaumasia and Hesperia Planae and Apollinaris Mons. We also selected a region to the east of Hellas (Eridania) which is composed of heavily eroded fluvial and volcanic material. More details on region selection can be found in section 1 of the Appendix.

Table 1: Average chemistry for each martian reference region, spatial extent in chemical map pixels, and geologic analog context for which they served as a reference. Underlying chemical data are the same as used in Figures 1 and 2. Values for SCR, BSCR and the martian crust are also given. The crustal proxy has SCR and BSCR removed to reduce sampling bias. Overall, our reference regions are close temporal counterparts to SCR. The mean mass fraction for K, Th, S and Cl is given for all the regions with K and Th reported in mg/kg and S and Cl reported as percentages (wt%). The ratios for K/Th and S/Cl are calculated from reported elemental weight percent. The 1 sigma error is the standard error of the mean; ratio error is calculated by $(K/Th)[(\sigma_K/K)^2+(\sigma_{Th}/Th)^2]^{1/2}$, where K and Th are the mean concentration of K, Th. The same applies to S and Cl.

Region Name	Geologic Analog	Age (Ga)	Average Elemental Abundance (K & Th in mg/kg, S & Cl in wt%) (1σ error)	
Hellas (48 Pixels)	Impact formed, Sedimentary Basin	~ 4.1	K: 3007 ± 145.2	S: 2.1 ± 0.3
			Th: 0.41 ± 0.06	Cl: 0.4 ± 0.04
			K/Th: 7325 ± 1138	S/Cl: 5.1 ± 0.8
Argyre (41 Pixels)	Impact formed, Sedimentary Basin	~ 4.0	K: 3021.6 ± 107.8	S: 1.9 ± 0.2
			Th: 0.49 ± 0.04	Cl: 0.38 ± 0.03
			K/Th: 6144.9 ± 601	S/Cl: 5.0 ± 0.7
Isidis (25 Pixels)	Impact Induced Magmatism	$\sim 3.9 - 3.8$	K: 3860.4 ± 120.6	S: 1.9 ± 0.2
			Th: 0.69 ± 0.05	Cl: $0.49 \pm .03$
			K/Th: 5625 ± 477	S/Cl: 3.9 ± 0.5
Eridania (14 Pixels)	Heavily Weathered Fine-Grained Material (multiple sources)	$\sim 4.0 - 3.7$	K: 3099 ± 92.4	S: 1.9 ± 0.3
			Th: 0.5 ± 0.04	Cl: 0.38 ± 0.03
			K/Th: 6190.2 ± 573	S/Cl: 5.1 ± 0.8
Thaumasia Planum (20 Pixels)	Volcanic Site	$\sim 3.8 - 3.7$	K: 2657 ± 67.3	S: 2.0 ± 0.2
			Th: $0.4 \pm .03$	Cl: 0.41 ± 0.03
			K/Th: 6581.5 ± 588	S/Cl: 4.9 ± 0.6
Hesperia Planum (12 Pixels)	Volcanic Site	~ 3.7	K: 2655.5 ± 81.5	S: 2.0 ± 0.2
			Th: 0.44 ± 0.04	Cl: 0.43 ± 0.03
			K/Th: 6035.2 ± 581	S/Cl: 4.7 ± 0.6
Apollinaris Mons (12 Pixels)	Volcanic Site	$\sim 3.6 - 3.8$	K: 3331 ± 104	S: 2.6 ± 0.2
			Th: 0.63 ± 0.05	Cl: 0.66 ± 0.04
			K/Th: 5325 ± 451	S/Cl: 3.9 ± 0.4
SCR (Arabia) (23 Pixels)	Proposed Volcanic Site	$\sim 3.9 - 3.8$	K: 3990.8 ± 117.6	S: 2.4 ± 0.3
			Th: 0.74 ± 0.05	Cl: 0.52 ± 0.04
			K/Th: 5372 ± 419	S/Cl: 4.6 ± 0.6
Broad SCR (Arabia) (48 Pixels)	Larger Region Housing SCR	$\sim 3.9 - 3.8$	K: 3684 ± 118.7	S: 2.3 ± 0.2
			Th: 0.69 ± 0.06	Cl: 0.49 ± 0.03
			K/Th: 5336.7 ± 460	S/Cl: 4.7 ± 0.6
Martian Crustal Proxy (1358 Pixels)	(Excluding SCR and Broad SCR)		K: 3523 ± 100.7	S: 2.2 ± 0.23
			Th: 0.61 ± 0.05	Cl: 0.46 ± 0.03
			K/Th: 5783.7 ± 474	S/Cl: 4.8 ± 0.6

526
527
528
529
530
531
532
533
534
535
536
537
538
539
540
541
542
543
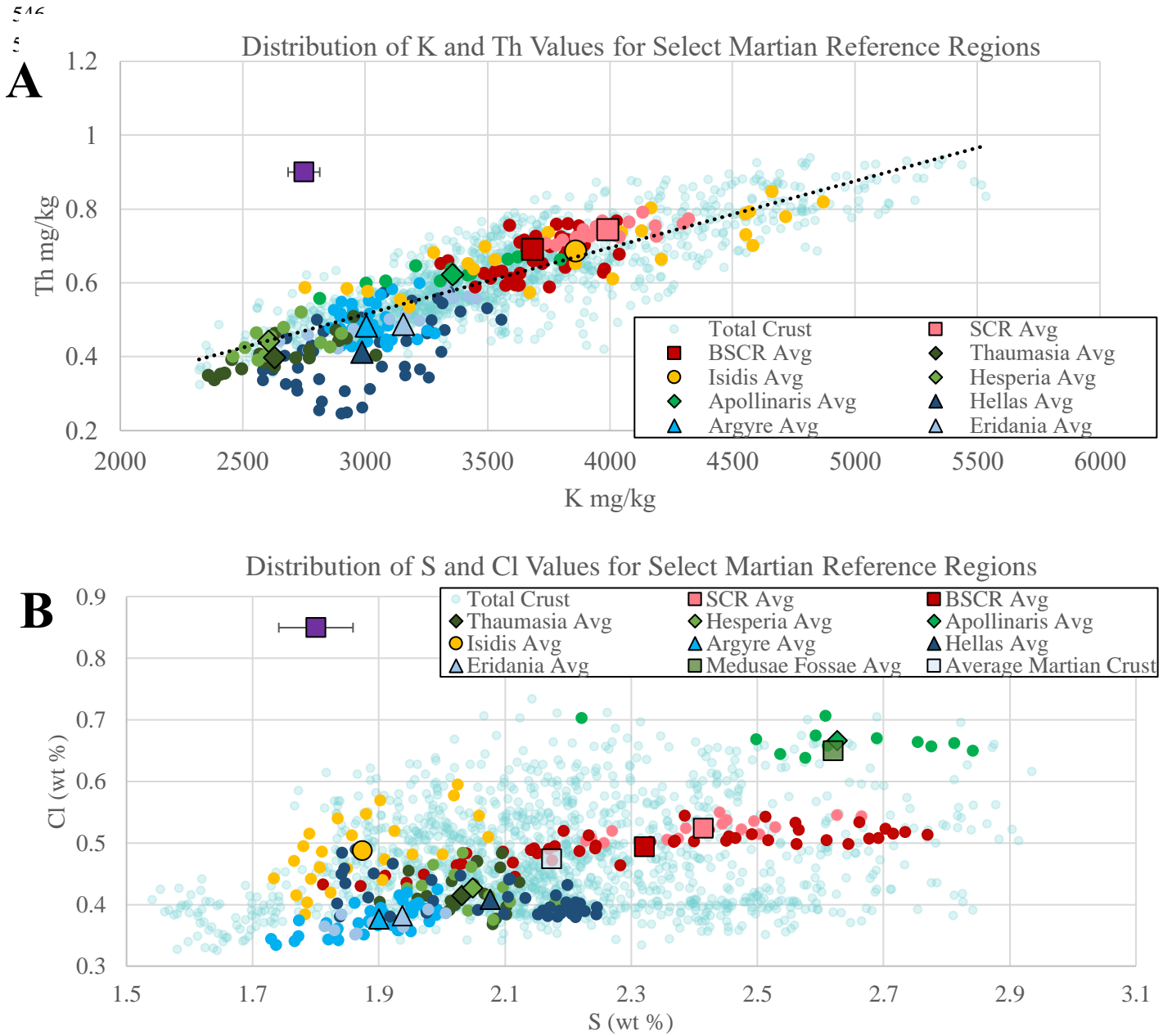544
545

546
5

A

B

Fig. 2: (A) Mean K and Th values (large polygons), along with the underlying data (small circles) used to calculate the mean for reference regions on Mars - and the mid to low latitudes - which show a linear trend as highlighted by the dotted line. SCR and BSCR are shown as squares, Isidis is represented by a circle, igneous references as diamonds and sedimentary references as triangles. Standard error for average values is displayed in top left as a purple square. Isidis, BSCR and SCR are grouped together at the higher end of observed K and Th abundances. SCR differs from Isidis in overall dispersion of K and Th abundances, with SCR having a much smaller dispersion in values. **(B)** Mean S and Cl values (formatting the same as in 2A), from chemical maps, along with the underlying data used to calculate the mean for reference regions on Mars, as well as S and Cl throughout the low to mid latitudes. MFF and Apollinaris Mons have the highest abundances of S and Cl, with SCR and BSCR reporting the second and third highest values, respectively. The remaining regions all have abundances lower than the crustal average. BSCR has a large dispersion in Cl values, much larger than what is observed for Apollinaris and SCR, both of which vary similarly. BSCR exhibits the largest range in values, whereas Apollinaris, Hellas, and SCR all show comparatively smaller range in S abundance. The remaining regions all exhibit abundances of S and Cl that are lower than the global average, and tend to cluster near each other, independent of provenance.
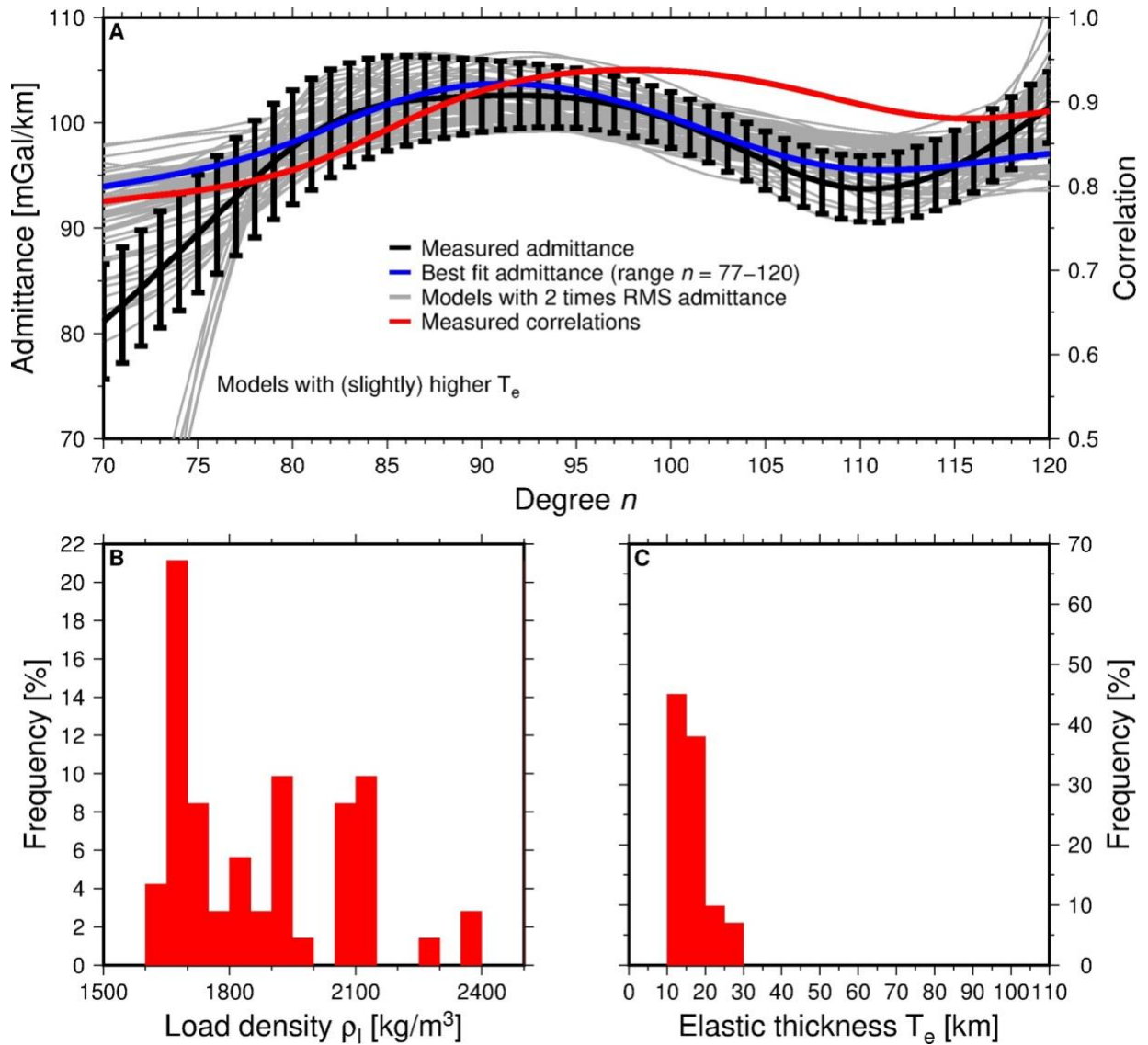
Fig. 3: Localized admittance and correlation between gravity and topography for the Arabia Terra area (centered on -5˚E,25˚N, for a spherical cap with a radius of 15˚), including the best-fit theoretical admittance and models within two times this best fit (**A**). **A** shows the best-fit admittance model of our geophysical analyses, which has a root-mean-square (RMS) of the misfit between the theoretical model and measured admittance of 1.34 mGal/km for our windowed region (SI Appendix, Fig. S3) (degree range 77-120). The error bounds on the admittance shown in Fig. 3A are computed from the relationship between admittance variance and correlation (Wieczorek, 2008). Histograms of the values for load density (**B**) and elastic thickness (**C**) for the models are also included.